AD-7/GBAR status report for the 2023 CERN SPSC

February 1, 2023

P. Adrich[1], P. Blumer[2], G. Caratsch[2], M. Chung[3], P. Cladé[4], P. Comini[5], P. Crivelli[2], P. Debu[5], A. Douillet[4,6], D. Drapier[4], P. Froelich[7], S. Guellati[4], P-A. Hervieux[8], L. Hilico[4,6], P. Indelicato[4], S. Jonsell[7], J-P. Karr[4,6], B. Kim[9], S. Kim[10], E-S. Kim[11], Y. Ko[9], T. Kosinski[1], N. Kuroda[12], B. Lee[10], H. Lee[10], J. Lee[9], E. Lim[11], L. Liszkay[5], D. Lunney[13], G. Manfredi[8], B. Mansoulié[5], M. Matusiak[1], V. Nesvizhevsky[14], F. Nez[4], S. Niang[13], B. Ohayon[2], K. Park[10], N. Paul[4], P. Pérez[5], C. Regenfus[2], S. Reynaud[4], C. Roumegou[13], J-Y. Roussé[5], Y. Sacquin[5], G. Sadowski[5], J. Sarkisyan[2], M. Sato[12], F. Schmidt-Kaler[15], M. Staszczak[1], K. Szymczyk[1], T. Tanaka[12], B. Tuchming[5], B. Vallage[5], D.P. van der Werf[16] D. Won[10], S. Wronka[1], Y. Yamazaki[17], K-H. Yoo[3], P. Yzombard[4],

(GBAR Collaboration)

[1] *National Centre for Nuclear Research (NCBJ), ul. Andrzeja Soltana 7, 05-400 Otwock, Swierk, Poland*
[2] *Institute for Particle Physics and Astrophysics, ETH Zurich, 8093 Zurich, Switzerland*
[3] *Department of Physics, Ulsan National Institute of Science and Technology (UNIST), 50, UNIST-gil, Ulsan 44919, Republic of Korea*
[4] *Laboratoire Kastler Brossel, Sorbonne Université, CNRS, ENS-Université PSL, Collège de France, Campus Pierre et Marie Curie, 4, place Jussieu, F-75005 Paris, France*
[5] *IRFU, CEA, Université Paris-Saclay, F-91191 Gif-sur-Yvette, France*
[6] *Université d'Evry-Val d'Essonne, Université Paris-Saclay, Boulevard François Mitterand, F-91000 Evry, France*
[7] *Department of Physics, Stockholm University, SE-10691 Stockholm, Sweden*
[8] *Université de Strasbourg, CNRS, Institut de Physique et Chimie des Matériaux de Strasbourg, UMR 7504, F-67000 Strasbourg, France*
[9] *Center for Underground Physics, Institute for Basic Science, 70 Yuseong-daero 1689-gil, Yuseong-gu, Daejeon 34047, Korea*
[10] *Department of Physics and Astronomy, Seoul National University, 1 Gwanak-Ro, Gwanak-gu, Seoul 08826, Korea*
[11] *Department of Accelerator Science, Korea University Sejong Campus, Sejong-ro 2511, 0019 Sejong, Republic of Korea*
[12] *Institute of Physics, University of Tokyo, 3-8-1 Komaba, Meguro, Tokyo 153-8902, Japan*
[13] *Université Paris-Saclay, CNRS/IN2P3, IJCLab, Orsay, France*
[14] *Institut Max von Laue - Paul Langevin (ILL), 71 avenue des Martyrs, Grenoble, France, F-38042*
[15] *QUANTUM, Institut für Physik, Johannes Gutenberg Universität, D-55128 Mainz, Germany*
[16] *Department of Physics, College of Science, Swansea University, Swansea SA2 8PP, United Kingdom*
[17] *Ulmer Fundamental Symmetries Laboratory, RIKEN, 2-1 Hirosawa, Wako, 351-0198, Saitama, Japan*

CERN-SPSC-2023-008 / SPSC-SR-324
01/02/2023

Abstract

We report on the activities performed during 2022 and the plans for 2023 for the GBAR experiment.

1 Introduction

Figure 1 depicts the presently installed parts of the experiment. Namely the positron beam produced with a linac followed by two traps for e^+ accumulation, the antiproton beam delivered by ELENA being further decelerated with a pulsed-drift-tube, and the proton source allowing to study

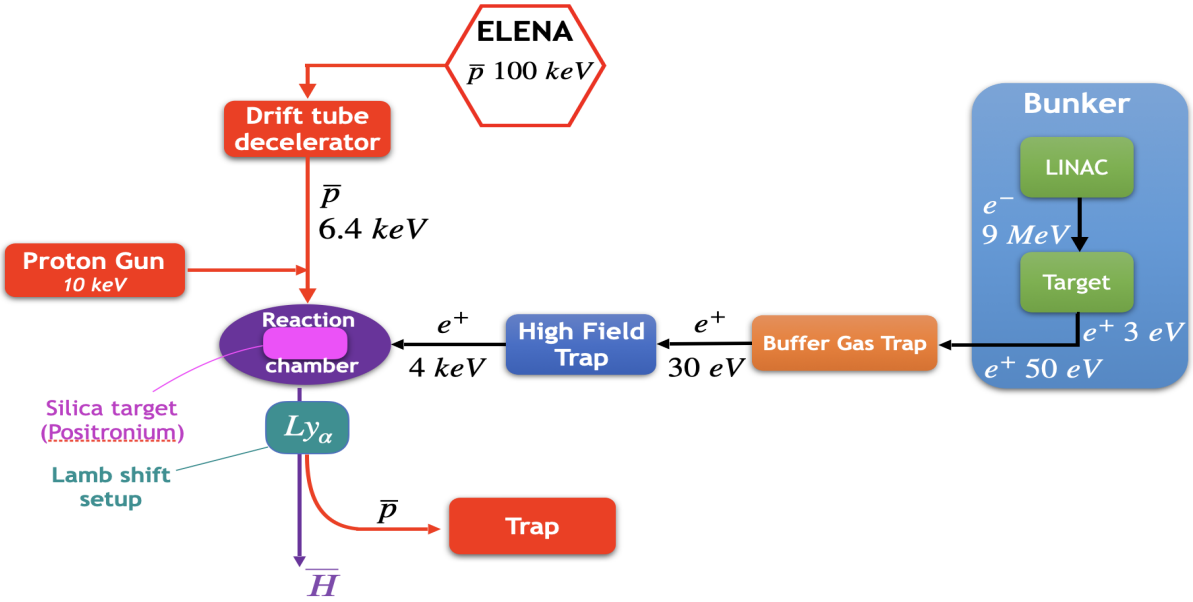

Figure 1: *Scheme of the present version of the GBAR experiment.*

the matter reactions with positronium. Those beams are focused to the same point where positrons are converted into positronium, which can be excited using a laser pulse. Hydrogen or antihydrogen atoms are transported to a dedicated setup to measure their Lamb shift. The outgoing charged

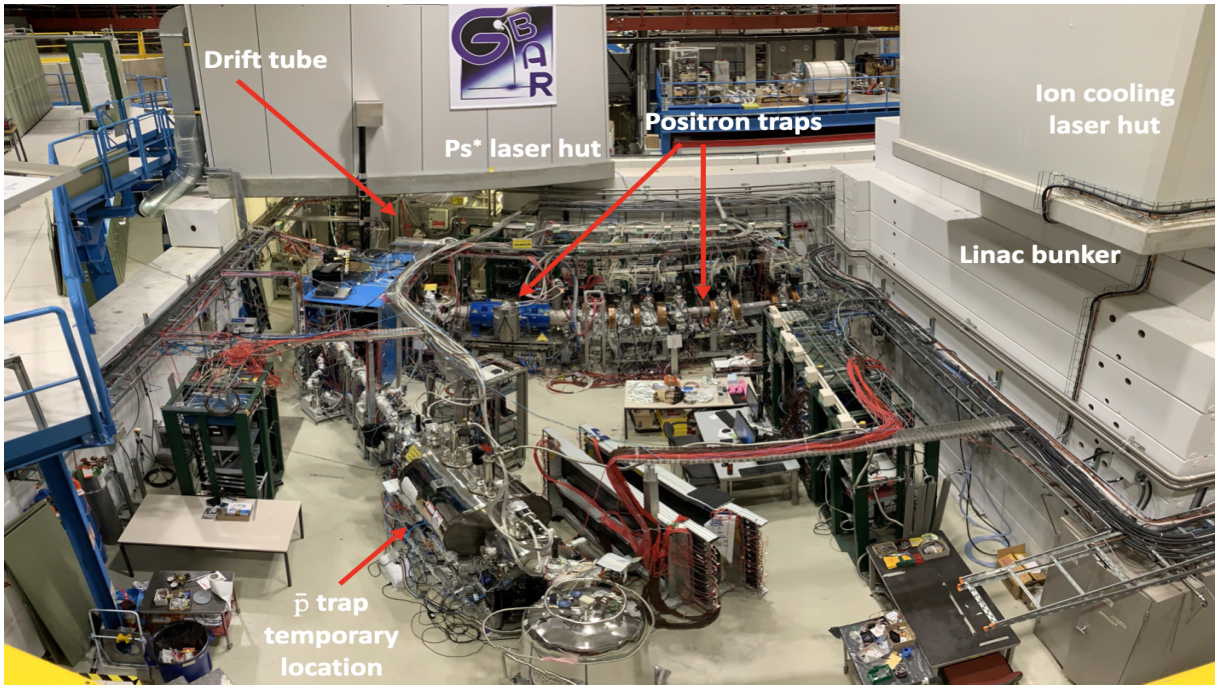

Figure 2: *Experimental zone.*

particles are separated employing an electrostatic switchyard. The chamber in which the free fall of anti-ions will take place is not yet made and is presently replaced by the antiproton trap, where it is tested before being transferred to its final position between the drift tube and the reaction chamber. Figure 2 shows the experimental zone.

2 Positron Production

The accelerating cavity of the linac [1] was replaced with a new, more efficient structure that worked as expected. However, failures in the equipment resulted in about two months without positrons. In particular the klystron supplying microwave power to the linac broke in October and was quickly replaced by a used device provided by NCBJ, rescuing the rest of the run for data taking. Inspection of the water cooled electron target showed small cracks on the tungsten structure. A new target has been prepared for quick replacement if needed.

Due to the problems encountered, we kept the linac power below the nominal value during the antiproton run. With the new klystron, at 120 Hz repetition frequency and with longer pulses, the positron flux was stable at 2.9×10^7 positrons per second. At full power we expect about 30% higher flux.

3 Positron trapping

Positrons are trapped in a series of two traps. The Buffer Gas Trap (BGT) captures and cools the positrons using N_2 and CO_2 (at 10^{-4} and 10^{-5} mbar respectively) while the High Field Trap (HFT) is able to accumulate them for long durations in a good vacuum [2]. During the 2022 run, we kept the performance obtained previously with a routine operation at 1.5×10^8 e^+ accumulated between two antiproton pulses.

We also pursue several tracks to increase the number of e^+ stored. For the BGT, in 2021 we tested a scheme where the N_2 gas is replaced by a solid SiC remoderator [3], however the location of the SiC plate did not allow transport to the HFT trap. In 2022 we started to study a new guiding mode, and in 2023 we plan to modify the electrodes geometry to enable the full implementation of this scheme. If successful, the efficiency of the BGT would increase from 10% with the present N_2 gas up to 40% with the SiC.

The capacity of the high field trap should also be increased. Although the density of the plasma before ejection is compatible with the best values found in the literature, we could not increase the length of the plasma while keeping the same density. Work is ongoing to improve the performances of this trap, for instance reducing the possible patch effect at the surface of the electrodes and improve hydrogen pumping. Also the drift tube used to accelerate particles at the ejection (from 300 eV to about 4 keV) will be extended to allow increasing the plasma length.

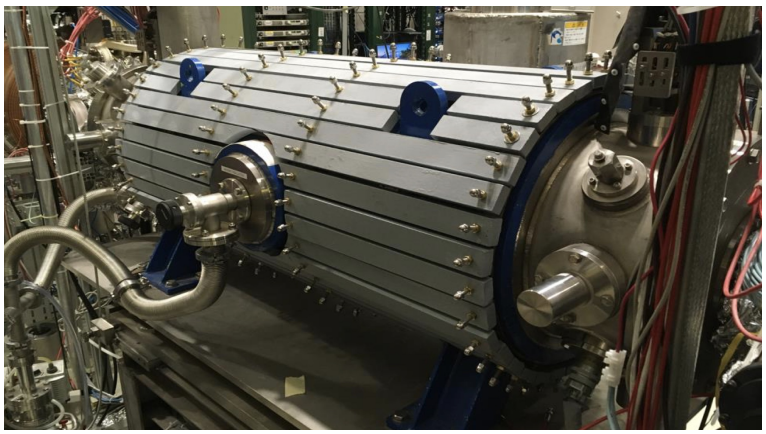

Figure 3: *High Field Trap (HFT). The grey iron bars increase the thickness of the return yoke.*

The fringe field of the HFT magnet influences the trajectory of the antiproton beam between the decelerator drift tube and the reaction chamber. The large blue box (see Figure 2) made of soft iron shields the zone close to the reaction chamber down to less than 4 Gauss. In order to reduce further this field we added thickness to the return yoke of the HFT in the form of iron bars surrounding it (Figure 3). The trapping performances were unchanged while the fringe field in the RC was reduced by a factor of two. Coils at the exit of the HFT were adapted for the transfer of positrons between the trap and the RC.

4 Positronium production

The accelerated positrons enter a region of low magnetic field inside the soft iron shielding (blue box), where the reaction chamber sits. Electrostatic lenses focus the positrons at the centre of the reaction chamber where different positron targets can be positioned to intercept the beam. Several detectors surround this zone (Figure 4). In particular a microchannel plate (MCP RC) is located inside the RC to image the beam spot and lead tungstate crystals (PWO and PWO2) detect gamma rays to produce single-shot lifetime spectra (SSPALS) to study positronium formation.

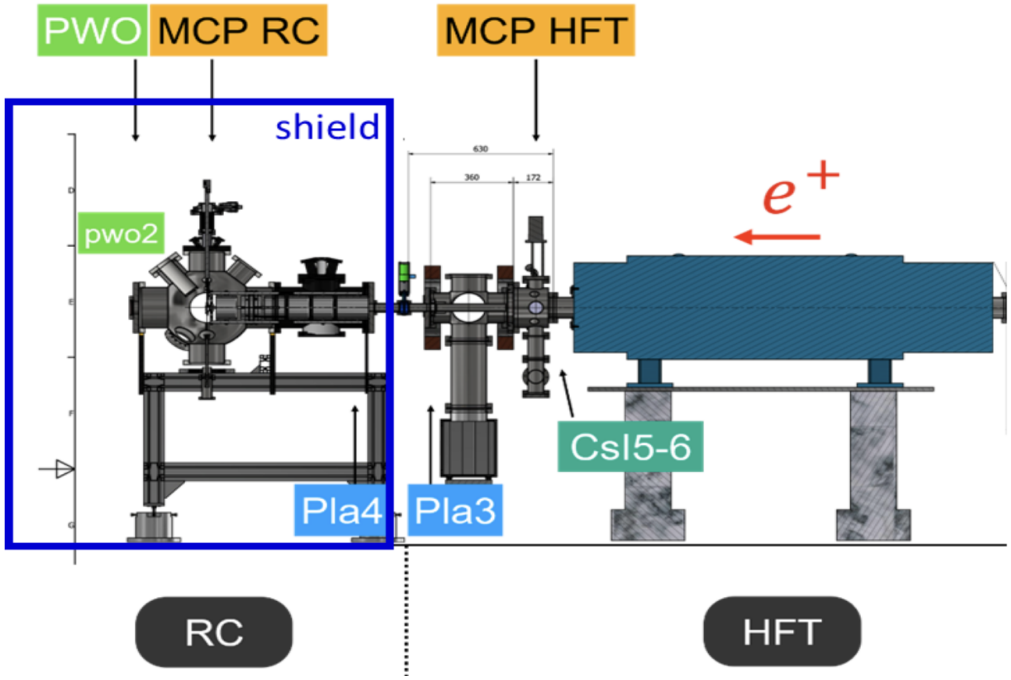

Figure 4: *Cut view of the end of the positron beamline, with the location of the different detectors. MCP RC has 10 mm diameter for imaging and 17 mm diameter for the measurement of the positron number reaching the interaction region by charge collection. The small lead tungstate crystal (PWO2) is placed at 100 mm from the target in a re-entrant well.*

The number of positrons reaching the centre of the reaction chamber last year was re-evaluated as 2.5×10^7 per ejection. In order to improve the transport, the lens system was upgraded with steerers to compensate for the asymmetric residual magnetic field. A refined tuning of the beamline allowed reaching a transport efficiency higher than 30 %, with typically 5×10^7 positrons on target for most of the beamtime. Thanks to an improved vacuum in the HFT and the implementation of a different ejection scheme, a record of 8×10^7 positrons on target was achieved in the last week of the beamtime (out of 1.8×10^8 from the HFT, that is more than 40% transport efficiency).

During the 2022 beamtime, GBAR used a plane Ps converter target (a 19×19 mm silicon plate coated with a nanoporous silica layer) and a simple silicon target for reference. From the PWO2 spectra, we estimate that about 18 % of the recorded annihilations are from the long-lived state of positronium. The expected yield of this type of converter for 4 keV positrons is around 20 %. From the mapping of the positron beamspot, we also estimate that 80 % of the emitted positronium overlapped with the antiproton beam. Out of the 5×10^7 positrons arriving on target, this gives 9×10^6 positronium atoms per spill, out of which about 7.2×10^6 positronium atoms participate in the antihydrogen production (and certainly more than 10^7 in the last days of beamtime).

The optimal scheme for the interaction of the $\overline{\mathrm{p}}$ and e^+ beams includes a small cavity ($2 \times 2 \times 20$ mm) where the Ps would be confined while the $\overline{\mathrm{p}}$ beam goes through. During the 2022 run, we found a transmission of $\overline{\mathrm{p}}$ through the cavity much lower than expected, for an unknown reason (probably a charge-up of some insulating part), hence we did not use it and we kept the flat target for $\overline{\mathrm{H}}$ production. This will be investigated and the cavity will be improved for this and for other features. The expected increase of the useful Ps number is 2 to 2.5.

5 Antiproton beam

We use a drift tube to decelerate the antiprotons to energies below 10 keV, suitable for producing antihydrogen $\overline{\mathrm{H}}$ [4]. This tube is held at more than 90 kV for 3 s before the antiproton bunch arrives, and is then switched to ground in less than 30 ns while the particles are traversing it. In 2022 ELENA provided a very good 100 keV $\overline{p}$ beam with a high availability. The typical intensity at the end of the run time as recorded by the ELENA beam monitor was between 1 and 1.2×10^7 $\overline{\mathrm{p}}$ per bunch (this number is currently being studied). Thanks to bunch rotation, the bunch length

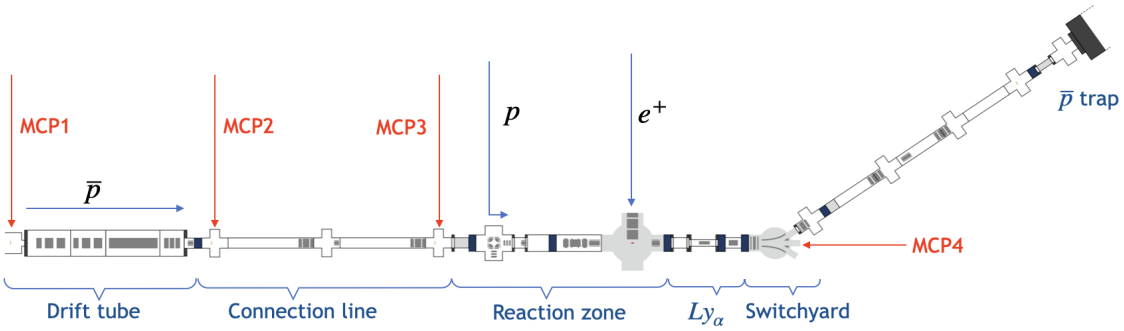

Figure 5: *GBAR $\overline{p}$ beam line in 2022. The $\overline{p}$ beam is decelerated by the drift tube, then focussed in the reaction chamber where it meets the Ps target to form $\overline{\mathrm{H}}$ atoms. After the reaction chamber an electrostatic Switchyard(SY) can deflect the $\overline{p}$ beam to the ion beamline, where the $\overline{p}$ trap is currently located. For the $\overline{\mathrm{H}}$ formation experiment, The SY and additional deflectors remove the $\overline{p}$s right after the reaction region, and neutral atoms are detected in MCP4 located in straight line downstream.*

was 40 ns (RMS), ensuring a complete containment inside our deceleration drift tube (DT), given also the small arrival time jitter of about 4 ns. The bunch rotation implies a doubling of the momentum spread, up to 2×10^{-3}, but this has a negligible impact for us. The horizontal and vertical emittances were carefully measured by the ELENA team as 2.9 and 2.1 μm (RMS) resp . These values are about 2.5 times larger than design, with a significant impact on the decelerated beam size and the possibility to focus it at the point of reaction with the Ps.

The stability and reproducibility of the $\overline{p}$ beam was excellent, from bunch to bunch and along the run period. ELENA also enabled the delivery of 100 keV H^- ions. However the position of this beam is affected by the field in the AD magnets, and hence it slightly varies along the AD cycle, making it difficult to use for an accurate beam adjustment. Together with the ELENA team, we might consider implementing steering corrections synchronized with the AD cycle, in order to provide a stable H^- beam to GBAR.

During the 2022 run, the DT was operated reliably at voltages above 90 keV (mainly 94 keV) with low leakage current, thanks to several improvements (removal of ion pumps, better cleaning of insulators, HV cable, etc.)

A SIMION simulation interfaced with COMSOL field maps is available which uses the 100 keV as fully characterized by ELENA, and models all the transport and focussing elements to the reaction chamber and beyond. The actual beam size was found to be larger than the simulated one, in particular at the reaction point, which was a limitation for $\overline{\mathrm{H}}$ production. Similarly, spurious deviations of the decelerated beam were observed, affecting beam steering and the precise knowledge of the neutral atoms trajectories.

Determination of the $\overline{\mathrm{p}}$ flux with a CMOS sensor

A study was performed to determine the number of antiprotons in the bunch at different locations in the beam line, with the help of a CMOS sensor mounted in a commercial BAUMER VCXG-51M camera (see Fig. 6 left). Due to the high number of pixels (5M) and large detection efficiency (close to 100%) the sensor can count reliably the number of traversing pions generated from $\overline{\mathrm{p}}$ annihilations on a surface. The number of antiprotons is inferred from the number of pions produced depending on the surface material [9] and the amount of material between the surface and the sensor (pion absorption, pair production,...). The uncertainty of the method is estimated to be around $\pm 20\%$. The number of antiprotons in 100 keV $\overline{\mathrm{p}}$ bunches annihilating on MCP3 was com-

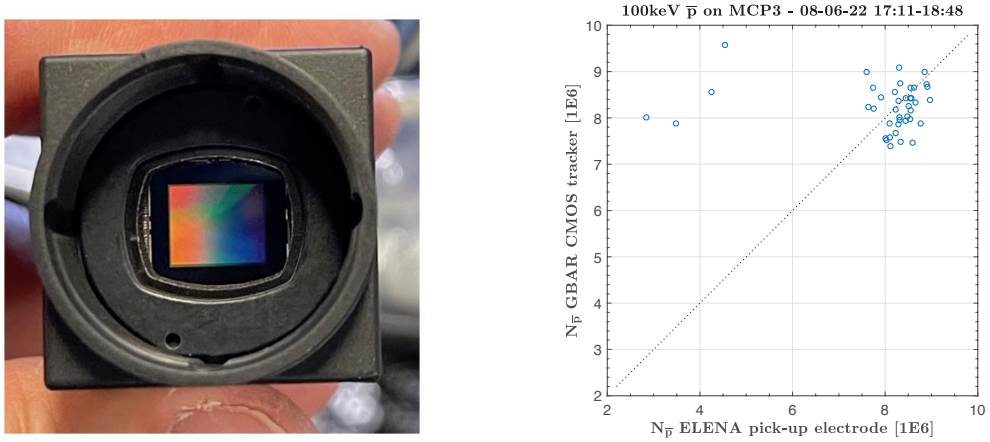

Figure 6: Left: Image of the CMOS sensor of the BAUMER VCXG-51M camera. Right: Comparison of $\overline{\mathrm{p}}$ numbers from the induction electrode from ELENA and the number of reconstructed tracks in the CMOS sensor.

pared to the value measured by the ELENA induction beam monitor in the early beam time (see Fig. 6 right). A fair agreement of both measurements can be observed. The main purpose of the CMOS detector is to estimate the amount of decelerated 6 keV antiprotons available at the target which pass the 5 mm diameter collimator and hence interact with the Ps cloud. This values was determined to be about 2.2×10^6 per spill from annihilations taken on MCP4 without deviating electric fields.

6 Combining $\overline{\mathrm{p}}$ and e^+ beams

The formation of $\overline{\mathrm{H}}$ by interaction of $\overline{p}$s with Ps is maximum at an incident energy of 6 keV [6] [7]. The concerted operation of the main components of the experiment to mix $\overline{\mathrm{p}}$ and Ps was achieved routinely during the fall of 2022. In the reaction chamber, the movable target holder allows to position two types of targets at the intersection of the $\overline{p}$ and e^+ beams: either a flat SiO_2 target facing the e^+ beam, or a cavity. For the flat target, the exiting Ps forms a free cloud in front of the target, while it is contained in the case of the cavity. Due to an unknown reason it was not possible to drive the correct amount of $\overline{p}$s through the cavity, hence only the flat target was used for the $\overline{\mathrm{H}}$ production experiment. Presently, the reaction is sequenced with the extracted bunches from ELENA, i.e. about every 2 minutes. Typically 5×10^7 e^+ were brought to the flat target, producing a cloud of 9×10^6 Ps. This cloud was traversed by about 2.2×10^6 $\overline{p}$, at the time optimal for the highest $\overline{\mathrm{H}}$ yield. Using the formation cross-section at these energies [6] [8], we estimate that 0.5 to 2 $\overline{\mathrm{H}}$ atom should be formed, every 100 crossings.

Once the beams are properly steered, voltages are applied to the deflectors right after the reaction area and to the SY electrodes, in order to deflect the $\overline{p}$s away. MCP4 located downstream on the beam axis is used to detect the $\overline{\mathrm{H}}$ atoms. The MCP electrical signal is short and accurate in time, and it should correspond to the expected time of flight of 6 keV $\overline{\mathrm{H}}$ atoms within the 40 ns bunch length. In contrast, the MCP also detects pions from annihilation of $\overline{p}$s upstream, but these occur mostly at earlier times, and with a more continuous time distribution. Most of the data taking time was shared between "Mixing runs", with the presence of both $\overline{p}$ and e^+ beams, and "Background runs", with only $\overline{p}$s, in order to estimate the background to $\overline{\mathrm{H}}$ in the Mixing runs. Indeed all the background is related to the $\overline{p}$ beam, and we checked that the background related to the e^+ beam is negligible. About 7000 shots of "Mixing" and 8500 shots of "Background" were recorded. The typical background in the relevant time interval for $\overline{\mathrm{H}}$s was about 0.8×10^{-3} per shot, which indicates that the detection of a significant $\overline{\mathrm{H}}$ signal is possible for the expected rate. The MCP image (Figure 7) can also provide information on the type of particle which originated the signal, although the image integrates over a much longer time of 1μs. Data were also taken with only pions or only $\overline{p}$s impinging on the MCP to help characterize the respective images. The analysis is currently ongoing.

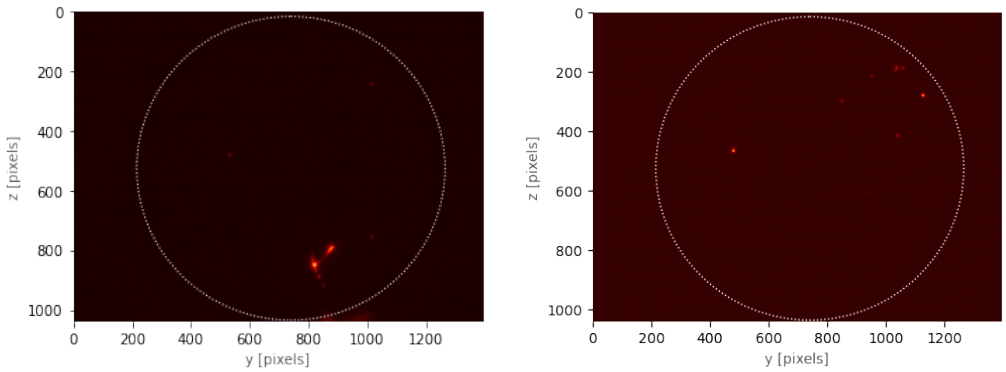

Figure 7: *Example image from the SY MCP for a mixing event (left) and for a background event (right).*

7 Antiproton trap

In 2022, the antiproton [5] trap was placed at the end of the beam line for commissioning studies, (Figure 5). The magnet, cooled with liquid Helium, can be operated up to 7 T with a 20 cm long region where the field gradient is less than a per mille, adequate for trapping. Its active shielding results in a negligible fringe field outside the upstream and downstream crosses. The central duct, hosting the electrodes is kept at cryogenic temperature using two cold heads (Figure 7). At the end of the run, a rough steering of the $\overline{\mathrm{p}}$ beam was performed for first studies. MCPs at the entrance and exit, and plastic scintillators were used for detection. The antiproton flux received from ELENA during these measurements was estimated at 9×10^6 per ejection, out of which 6% reached the trap entrance cross and 40% entered the trap, i.e. of the order of 2×10^5. The measured trapping efficiency varied between 40 and 70% with 20% error depending on the trap length used. At 5 T with $\approx 10^7$ electrons and 10^5 antiprotons trapped the cooling time was 3.6 s. At 10^{-10} mbar the lifetime was ≈ 30 s. The incoming beam quality and stability, as well as the residual pressure must be improved in order to study more precisely and improve these performances.

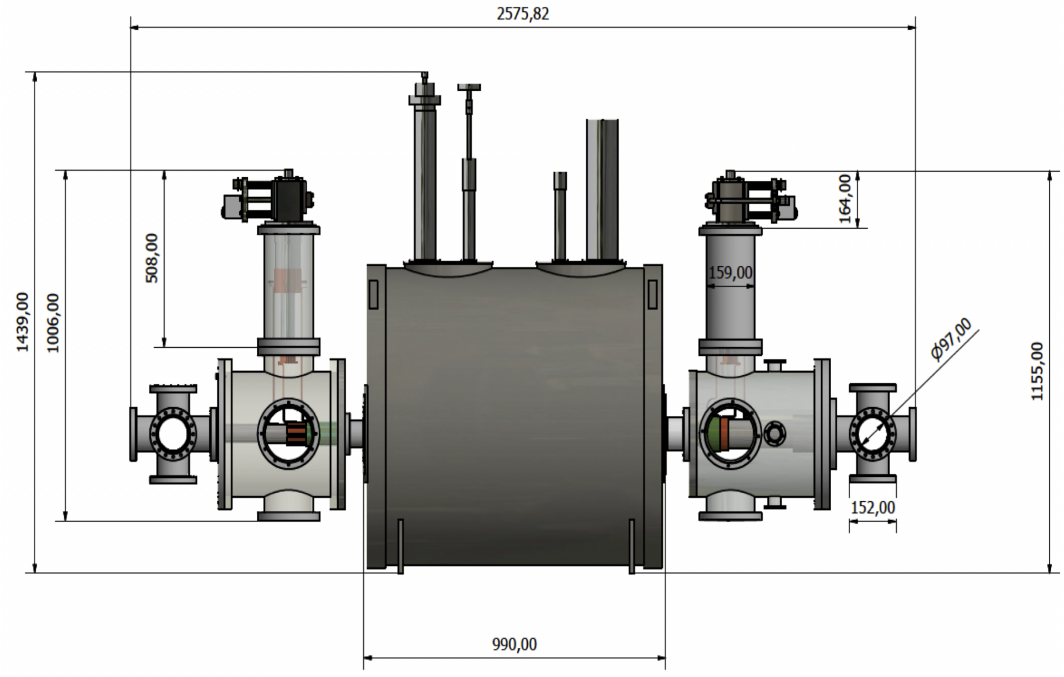

Figure 8: *Side view of the antiproton trap.*

8 Activities in the collaborating institutes

In the home laboratories, activity is oriented toward the next steps of the experiment.

The ESPRIT (Exploring stopping power in ion traps) [10] project is studying the kinetic energy transfer from an incoming charged projectile to an ion cloud target to prepare the capture step of a fast $\overline{\mathrm{H}}^+$ ion in the GBAR experiment. There is a continuing effort in the study of the $\mathrm{Be}^+/\mathrm{Sr}^+$ sympathetic cooling. The development of the photo detachment laser is being pursued and a prototype is currently being developed [11]. Magnetic probes are being developed to be implemented in the GBAR zone to diagnose eventual fluctuations of the ambient magnetic field that would affect the antihydrogen transport. The possibility of diagnosing antihydrogen production on the reaction chamber target via monitoring x-ray emission from antiprotonic atom cascades is also being pursued, as well as a solution for antiproton recycling to improve the antihydrogen yield. The technique of polarisation gradient cooling of ions has been improved in robustness and noise level [12]. The SPHINX project (for "study of positronium-hydrogen interactions: negative hydrogen production cross sections") [13], promotes a physics application of the H^- beam provided by ELENA. From this beam delivered in between antiproton pulses, the project intends to form a beam of neutral hydrogen and use it to measure cross sections for the reaction $\mathrm{H} + \mathrm{Ps} \rightarrow \mathrm{H}^- + \mathrm{e}^+$, the charge conjugate reaction of $\overline{\mathrm{H}}^+$ formation. In 2023, the focus is on the integration to the GBAR set-up and on the neutral beam preparation.

On the theoretical side, there are calculations of relevant cross-sections [14] and studies of the quantum interference measurement of the free fall of anti-hydrogen [15].

9 Outlook

At the end of the 2022 run, routine operation of the decelerated antiproton beam and positronium production allowed to attempt measuring the production of antihydrogen via the first charge exchange reaction foreseen in the GBAR proposal. A preliminary analysis of the recent data strongly suggests the presence of this production. While analysis is still ongoing, we are preparing for the 2023 run. The main goals are to improve the performances of the incoming beams to the reaction zone in order to increase the production rate of antihydrogen atoms and to advance toward the detection of the Lamb shift transition.

In 2023 the linac should reach full power. With the new trapping scheme using SiC, and possible improvements on the transfer efficiencies between devices this may increase the number of accumulated positrons by a factor 5. With the antiproton trap we expect improved steering allowing to use the small Ps confining cavity. Altogether this would bring a factor 100 increase in the production rate, i.e. up to 1 $\overline{\mathrm{H}}$ per shot.

With all the improvements foreseen for 2023, we estimate that 5 $\overline{\mathrm{H}}$ atoms per hour will be produced in the 2S state. Such a rate would allow commissioning of the Ly-α setup and preparing for a Lamb shift measurement. A study of the antihydrogen production cross section as a function of energy may also be performed.

Other improvements are under scrutiny that may bring more flux toward producing anti ions. For instance the moderation of positrons by adapting a cyclotron trap [16] or using solid Neon may enhance the slow positron yield by a factor 2 to 3. The SiC based remoderation step in the BGT could be further increased by a factor 2 if placed at a different location. If steering of the beams is also improved the section of the reaction cavity could be reduced down to the 1 mm x 1 mm size quoted in the proposal, increasing the Ps density by a factor 4. The trapping efficiency for antiprotons should also improve with time.

The design study using a quantum interference method as in [15], shows that more information is usable than in the classical technique, leading to three orders of magnitude increase in precision with the same statistics.

Acknowledgements

We thank F. Butin and the EN team, L. Ponce and the AD/ELENA team for their fruitful collaboration. A. Prost and T. Stadlbauer are also warmly thanked for their help on HV techniques for the decelerator as well as A. Sinturel for help and expertise on vacuum.

References

[1] M. Charlton et al., Nuclear Inst. and Methods in Physics Research, **A 985**, 164657 (2021).

[2] P. Blumer et al., Nuclear Inst. and Methods in Physics Research, A **1040**, 167263 (2022).

[3] A.M.M Leite et al., Journal of Physics: Conf. Series **791**, 012005 (2017).

[4] A. Husson et al., Nuclear Inst. and Methods in Physics Research, **A 1002**, 165245 (2021).

[5] Kyoung-Hun Yoo et al., JINST **17**, T10003 (2022).

[6] C.M. Rawlins et al., Physical Review **A 93**, 012709 (2016).

[7] P. Comini, P-A. Hervieux and K. Lévêque-Simon, Corrigendum: New J. Phys. **23** 029501 (2021).

[8] K. Lévêque-Simon, PhD Thesis, University of Strasbourg, France (2020); P. Comini, PhD Thesis, Université Paris VI, Pierre et Marie Curie, France (2014).

[9] G. Bendiscioli, D. Kharzeev, Riv. Nuovo Cim. **17**, 1 (1994).

[10] ESPRIT, French ANR funded project, ANR-22-CE30-0028-01.

[11] PHOTOPLUS, French ANR funded project, ANR-21-CE30-0047.

[12] W. Le et al., New J. Phys. **24**, 043028 (2022).

[13] SPHINX, French ANR funded project, ANR-22-CE31-0019-01.

[14] T. Yamashita et al., Phys. Rev. A **105**, 052812 (2022).

[15] O. Rousselle et al., Eur. Phys. J. D **76**, 209 (2022).

[16] L. Gershow et al., Instruments **2**, 10 (2018).